SSEC No.84.04.X1

Science and Engineering Center
University of Wisconsin-Madison

Satellite Microwave Observations of the Gobi Desert of China

A REPORT from the

Cooperative
Institute for
Meteorological
Satellite
Studies

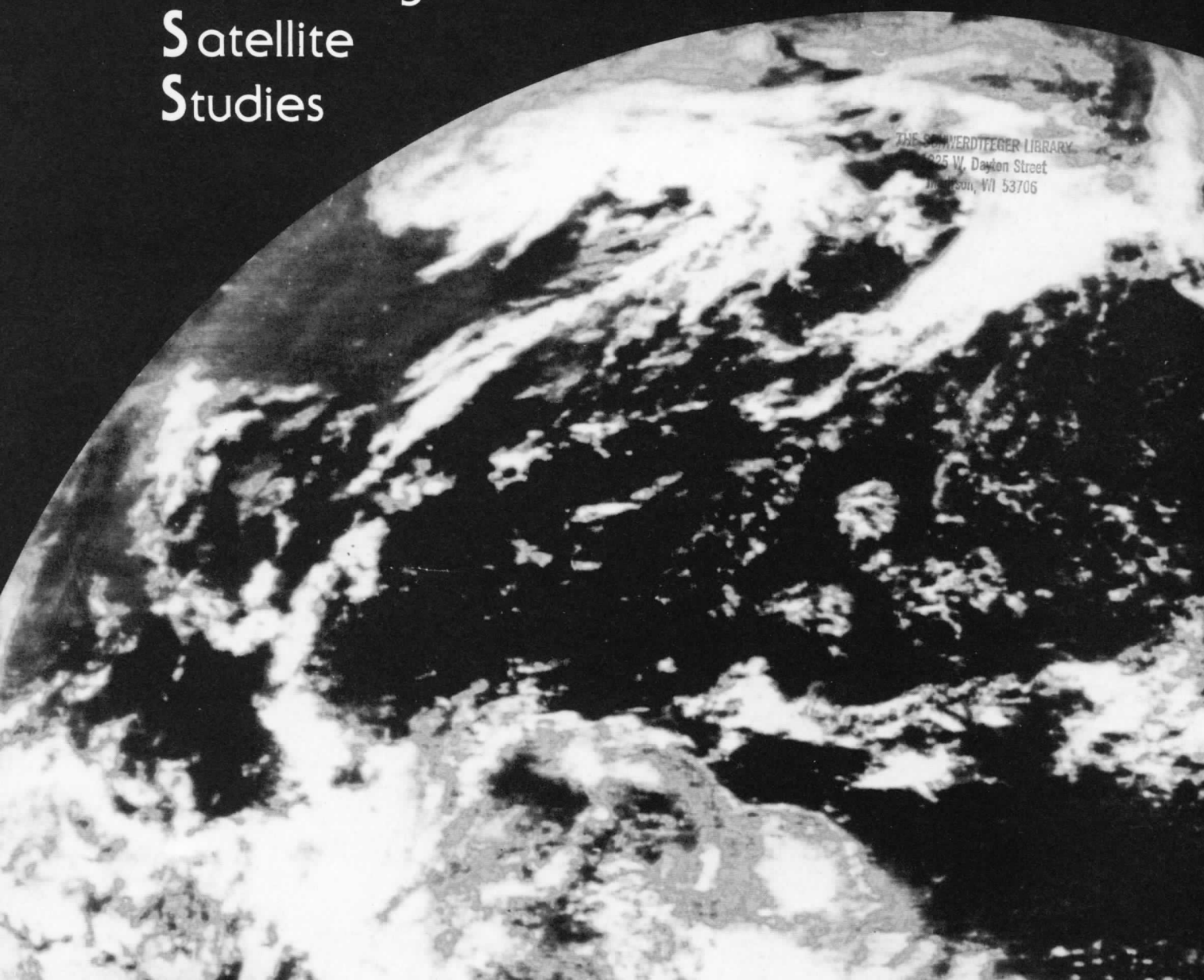

THE SCHWERDTFEGER LIBRARY
1225 W. Dayton Street
Madison, WI 53706

A Report to

NATIONAL ENVIRONMENTAL SATELLITE DATA AND INFORMATION SERVICE
NATIONAL OCEANIC AND ATMOSPHERIC ADMINISTRATION

for

Satellite Microwave Observations of the Gobi Desert of China

Jointly Supported by NOAA Contract NA-80-SAC-00742

and The Cooperative Institute for Meteorological Satellite Studies

for the period of

1 April 1983 to 1 April 1984

submitted by

Xu Xi
Roy W. Spencer

Xu Xi

Space Science and Engineering Center
University of Wisconsin-Madison
1225 West Dayton Street
Madison, Wisconsin 53706
(608) 262-0544

April 1984

ABSTRACT

This report summarizes the work performed by Mr. Xu Xi during part of his stay at SSEC as a visiting scientist from the Satellite Meteorological Center of the National Meteorological Bureau, Beijing, Peoples' Republic of China. Investigated was the unusual radiative signature discovered in the Gobi Desert at the passive microwave frequencies of 37, 21, 18, 10.7, and 6.6 GHz. This signature had the form of a multispectral contrast in brightness temperature (T_B), with the 37 GHz T_B's markedly lower than those of the lower frequencies. This signature is typical of rain systems and other geophysical phenomena involving the preferential scattering of upwelling radiation at the shorter wavelengths by particles having sizes comparable to the wavelength of the sensed radiation, and is attributed to the scattering by pebbles and gravel which occur in the Gobi Desert in great abundance.

Acknowledgements

I wish to express my appreciation to Professor V.E. Suomi and Executive Director R.J. Fox for making it possible for me to be at the Space Science and Engineering Center (SSEC) during 1982-1984. My visit to SSEC also gave me the opportunity to use the facilities and data in several fields at the University of Wisconsin.

The content described in this report was developed with the close cooperation of Dr. Roy Spencer and Dr. David Martin. Dr. Alta Walker provided maps and samples of rock from the Gobi Desert. I thank Mr. David Santek for his invaluable assistance on McIDAS. The manuscript was typed by Angela Crowell and Joanne Edwards.

I also appreciated the cooperation of Ms. Lynda Parker, the Administrator of Services at SSEC.

Finally, but most important, I thank all the members of SSEC for their help.

Table of Contents

1. INTRODUCTION

A passive microwave remote sensing technique for the measurement of rainfall in agricultural areas has been described by Spencer et al. (1983). Upwelling radiance was determined using the Scanning Multichannel Microwave Radiometer (SMMR) flown aboard Nimbus-7. Correlations between SMMR brightness temperatures at 37, 21, 18, 10.7, and 6.6 GHz and radar rain rates were made by a stepwise regression procedure. The study showed that the rain rate is primarily related to the contrast in brightness temperature (T_B) betwen the 37 GHz channels and the lower frequency channels of the SMMR. The difference in signs between high frequency coefficients and low frequency coefficients implies a sensitivity of rainrate to contrast in brightness temperature between the land background and the rain cells. The lower the 37 GHz T_B's are below the 21 GHz (or 18 GHz, etc.) channel T_B's, the greater the measured rain rate typically is.

It is very important to investigate the passive microwave characteristics of the land backgrounds of different geographic areas (e.g. mountains, deserts, forests) to determine their brightness temperature and polarization signatures in the frequencies observed by the Nimbus-7 SMMR instrument. Then, these signatures can be compared to those observed over the United States for which the University of Wisconsin (UW) microwave rain estimation algorithm was developed. This will help determine the global applicability of this algorithm.

2. GLOBAL RAIN ESTIMATION - THE GOBI ANOMALY

Spencer et al. (1983) has shown that the rain rate, R, can be derived from the SMMR microwave brightness temperatures T_B through the relationship

$$R = 32.7 - .363V37 - .414H37 + .172V21 + .200\ H21 + .116V18 + .385H18 - .214H10.7 \quad (mm\ h^{-1}), \tag{1}$$

where V37 represents the vertically polarized 37 GHz T_B(K), etc. The difference in sign between the 18 and 21 GHz and the 37 GHz terms reflect the dependence of the computed rain rate on the contrast in T_B between these frequencies. Both rain attenuated and land background information are contained in the brightness temperatures at all frequencies, but the 37 GHz channel is more affected by rain than any other channel, while that effect diminishes as the wavelength increase and the effect of land correspondingly increases. The estimate of rainfall is based upon the extent to which the radiation from land is attenuated by the rain.

Based upon global SMMR data between 21 June and 13 July 1979, algorithm calculated rain rates greater than 5 mm h^{-1} were printed out on the University of Wisconsin's Man-computer Interactive Data Access System (McIDAS), with "Cell 2" gridded data of 90 km resolution. Brightness temperature polarizations between the vertical and horizontal 37 GHz averages that were less that 15°C, (standing water or wet soil) were ruled out. The most obvious "false rain" signatures occurred in the Gobi Desert extending from 90°E to 110°E and 40°N to 46°N and the Arctic Ocean at midnight (Fig. 1). This phenomenon in the Gobi Desert is surprising because this zone is known to be desert, barren land with meager rainfall that can support only sparse vegetation and a limited population. This finding led to the following investigation into the possible reasons why the Gobi Desert has a multi- spectral microwave signature similar to that of rainfall.

3. WEATHER CONDITIONS IN THE GOBI DESERT

3.1 Climatic characteristics of the Gobi Desert

The Gobi Desert is comprised of the western Hexi corridor, southern Tian Shan, Eastern Turpan Depression, Northern Aerchin Shan, and is one of the Hyperarid zones of China (Fig. 2). This zone has an annual precipitation of between 10 and 30 mm. (Zhu et al., 1980). In addition, soil maps of north and central Asia indicate that the Gobi Desert, an absolute warm continental desert, has 1120 mm of annual potential evapotranspiration, zero leaching rainfall, 1040 mm of drought stress, and no humid season. (FA-UNESCO soil map of the world, volume III).

3.2. Conventional weather station data

Data from four conventional weather stations in the Gobi Desert, during satellite data coverage, were extracted from computer tape storage, showing different weather phenomena. As mentioned before, rain rates greater than 5 mm h^{-1} were printed out from the University of Wisconsin's Man-computer Interactive Data Access System McIDAS. However, the four stations' data indicated that precipitation was seldom observed. Even though there was rainfall at a station, its rain rate was less than 5 mm h^{-1}. Therefore, we can conclude that the Gobi Desert calculated rainfall was a "false rain" signature.

4. RELATIONSHIP BETWEEN U.S. RAIN AND GOBI "FALSE RAIN"

A stepwise discriminant analysis procedure was used to discriminate "Gobi" vs U.S. rain (Spencer et al., 1983). It was found that, respectively, the Gobi and U.S. rain classification functions are as follows:

$$\text{U.S. rain (classification function)} = -3.49(V37) + 9.5(V21) + 4.58(H21) - 1.18(H18) - 0.10(V10) - 0.16(H10) + 8.59\,(V37 - H37) - 1266 \qquad (2)$$

Gobi (classification function) = -3.64(V37) + 8.46(V21) + 6.00(H21) - 2.39(H18) + 1.20(V10) - 0.76(H10) + 7.18 (V37 - H37) -1194 (3)

For a given set of T_B's, that function with the larger value represents the class to which the data belong. These two functions allow a 97% separation between the U. S. rain and Gobi false rain signals. Similarly, false rains computed over Arctic ice fields were separable from the U. S. rains with 97% accuracy. These functions take into account the fact that the absolute values of the SMMR T_B's are different for rain than they are for the Gobi Desert, whereas the computed rain rate in Eq. 1 is heavily dependent upon the measured differences in T_B's between frequencies. Even though it is possible to separate these two signals, it is still of considerable interest to know what causes the differences in T_B between frequencies.

5. MICROWAVE IMAGES

Multifrequency microwave images of the Gobi region at midnight and noon were displayed on McIDAS. Different frequency microwave images displayed on the TV screen should reflect different physical aspects of the desert. The false rain in the Gobi was the result of a temperature contrast between the 37 GHz brightness temperatures and the lower frequency SMMR brightness temperatures. Specifically, the 37 GHz T_B's were typically 5°-10°C colder than the 21 GHz or 18 GHz T_B's (Fig. 3 a-e). In a rain situation the lower frequencies provide information on the land background (unattenuated) radiation while the 37 GHz channel variations in T_B are primarily the result of rain activity. In the Gobi, however, the lack of rain suggests that the desert surface material has a significantly different signature at 37 GHz from that at the lower frequencies. The basic goal in explaining this unusual radiometric signature is to interpret radiometric measurements obtained at various wavelengths and polarizations

in terms of geophysical parameters, where each of the channels is sensitive to several parameters, but to different degrees.

In the SMMR 37 GHz image, the red (green) shades stand for warmer (colder) T_B's. At 37 GHz, the Gobi Desert is colder than the Taklimakan Desert. However, at, say, 10.7 GHz the T_B's are roughly the same. The T_B's from all the SMMR channels are a function of the radiation emerging from the earth surface modified by the intervening atmosphere. Because 37 GHz is a microwave window channel, its microwave image represents the relationship between the surface emissivity and the surface thermodynamic temperature. However, 21, 18, 10.7 and 6.6 GHz frequencies provide information from increasingly deep soil layers. A disadvantage commonly encountered with the use of lower frequencies is the relatively coarse surface resolution that is obtained from the satellite. The footprint size increases linearly with wavelength. The 21 GHz channel is sensitive to water vapor, but this effect can be neglected in the dry desert air conditions. The lower frequency images shown might represent some subsurface differences in thermometric temperatures.

Fig. 4 shows microwave images of simplified rain estimation parameters. From an analysis of the coefficient sizes in the Spencer et al. (1983) algorithm, we know that the 37, 21, and 18 GHz T_B differences are the major reasons causing false rain phenomena in the Gobi Desert, e.g. the calculated rain rate increases as (V21-V37) becomes larger.

In order to quantitatively compare the Gobi Desert brightness temperature condition with other regions, we made two cross-sections along 41°N and 92°E (Fig. 5). Brightness temperatures at midnight showed that 37 GHz brightness temperatures in the Gobi Desert are lower than those in the

sand desert. However, at noon, this situation is not as strong, implying some diurnal thermal effects. We must further examine these features in order to find possible reasons for the surface brightness temperature anomalies.

6. GEOPHYSICAL CONDITIONS IN THE GOBI

All factors influencing surface brightness temperature anomalies and their measurement must be considered, e.g. soil type and thermometric temperatures, soil and air moisture content, and soil emissivity.

6.1 Relative humidity calculations

Relative humidity was calculated using ten ground weather stations data of shelter height temperature and dew point during 21 June to 30 July to show average values for daytime vs. midnight. The Gobi T_B anomaly is not attributable to the change in the surface emissivity caused by presence of dew on the Gobi Desert because the air temperatures did not become low enough to cause appreciable condensation.

6.2 Surface emissivity calculation

The emissivity of nonvegetated land surfaces can vary from 0.85 to 0.95 and, depending on the soil moisture content, the occurrence of dew, the surface temperature, and receiver polarizations, can indicate microwave brightness temperature between 205 and 310 K. Surface microwave radiance can be affected by roughness, topographic slope, stratigraphy (layering of different materials), density of rocks, vegetation, receiver wavelengths, and angle of incidence observed (Allison, 1977).

The microwave radiance emitted from the earth's surface is given by $T_B = \varepsilon T_s$, where ε is the surface emissivity and T_s the surface

thermodynamic temperature, provided here by the Nimbus-7 Temperature-Humidity Infrared Radiometer (THIR) in the 10.5 to 12.5 μm "window region".

Njoku et al. (1977) demonstrated that most data interpretation to date has made use of emissivity or radiative transfer models to describe the effect of medium properties on the emitted radiation. The emissivity approach and radiative transfer models are especially questionable for the longer wavelengths and greater sensing depths.

However, the equation "$T_B = \varepsilon T_s$" is a good approximation to the brightness temperature when the vertical temperature profile is essentially constant over the sensing depth. Thus at the higher frequencies where the radiation arises from within a region close to the surface, "$T_B = \varepsilon T_s$" is often used. At longer wavelengths and correspondingly greater sensing depths, this equation becomes decreasingly accurate.

After the differences between the ground resolution of the high resolution 11.5 um channel (7 km at nadir) and the SMMR channel (22 km) are considered, calculations showed that the 37 GHz emissivity ($=(T_B^V + T_B^H/2T_s$) of the Gobi false rain region under clear sky is approximately 0.88. It is observed that this lower emissivity of the Gobi false rain region is a major reason for the surface 37 GHz brightness temperature anomalies.

6.3. Geological conditions in the Gobi

Allison (1977) demonstrated that some observations of lower emissivity (0.7) in the Middle East resulted from limestone deposits. Walker (1982) noted that 43% of Chinese desert land, located in western and north central China along the fringes of the major basin deserts, throughout the Hexi corridor, and on the plains north of the corridor, consists of Gobi--loose,

unsorted gravels predominantly of pebble size (4-64 mm in diameter). Generally, if more than 50% of an area is gravel or cobble plains, it is referred to as a "gobi" desert (Fig.2).

It is difficult to explain the relationship between false rain and local geological signature, except to say that most of the false rain is in the Gobi Desert. Therefore, we attempted to apply modified rain algorithms to the highest resolution SMMR data (20 km) over a subregion of the Gobi where false rain was prevalent.

The rain rate (computed) is proportional to the difference between the 37 GHz T_B's and the 21 GHz or 18 GHz T_B, so these differences were displayed as images on McIDAS (Fig. 6) over a small part of the Gobi Desert. Dark areas in these images show regions where the differences in T_B between frequencies are essentially zero, and can be traced on a soils map (Fig. 2) to areas of sand, alkaline soils mixed with sand, or mountainous regions having some vegetative cover. The brighter regions are those composed of gobi (gravel, pebbles), and represent T_B differences of up to 10°C.

6.4 The hypothesized false rain mechanism

There are different size diameter gravels in the Gobi Desert. Scattering is a physical process by which a particle (such as a pebble) in the path of an electromagnetic wave continuously abstracts energy from the incident wave and reradiates that energy in all directions. Therefore, the various gravels of the Gobi Desert may be thought of as point sources of scattered energy. The relative intensity of the scattering pattern depends strongly on the ratio of particle size to wavelength of the incident wave.

As already noted, the SMMR aboard Nimbus-7 measures thermal radiation upwelling from the earth's surface and the intervening atmosphere at five frequencies 37, 21, 18, 10.7, and 6.6 GHz. These frequency wavelengths respond to 0.81, 1.36, 1.66, 2.8, 4.54 cm respectively.

The Gobi Desert has many gravel particles in the 0.81 cm range. These probably act as strong scatterers of 37 GHz radiation, leading to cold 37 GHz T_B's. At the lower frequencies (longer wavelengths), the pebbles have less effect on the upwelling radiation, and thus the brightness temperatures are higher. At the lower frequencies (longer wavelengths), the pebbles have less effect on the upwelling radiation, and thus the brightness temperatures are higher.

7. REQUIRED FUTURE WORK

This "false rain" which occurred in the Gobi Desert at midnight in summer is a very interesting science problem covering meteorology, geology, hydrology and other disciplines. Suggested future work includes:

1. Investigation of the passive microwave characteristics of different geographic areas to determine their brightness temperature and polarization signatures in the frequencies observed by the Nimbus-7 SMMR instrument in winter, as well as summer.
2. Update radiative transfer models to describe the effect of the land background.
3. If possible, the Gobi Desert should be investigated by visiting those regions of the Gobi with the strongest and weakest rain signatures, and comparing their respective gravel sizes, shapes, and number densities.

References

Spencer, R. W., D. W. Martin, B. B. Hinton, and J. A. Weinman, 1983: Satellite Microwave Radiances Correlated with Radar Rain Rates over Land. Nature, 304, 141-143.

Zhu, Z. D., Wu Z., and Liu S. 1980: Zhongguo shamo Gailun [General Introduction to China's Deserts]. Beijing: Science Publishing House. In Chinese. (from Dr. A. Walker).

FA-Unesco soil map of the world, volume III.

Allison, L. J., 1977: Geological Applications of Nimbus Radiation Data in the Middle East. NASA Technical Note NASA TN D-8469.

Njoku, E. G., Jin-Au Kong, 1977: Theory for Passive Microwave Remote Sensing of Near-surface Soil Moisture. Journal of Geophysical Research, 82, 3108-3118.

Walker, A., 1982: Deserts of China. American Scientist, 70, 366-376.

8/RS3/1

Fig. 1 "False rain" signatures computed from the microwave rain estimation algorithm from SMMR coverage at midnight from June to July 1979, in the region from 40^{o} - 46^{o}N and 90^{o} - 100^{o}E.

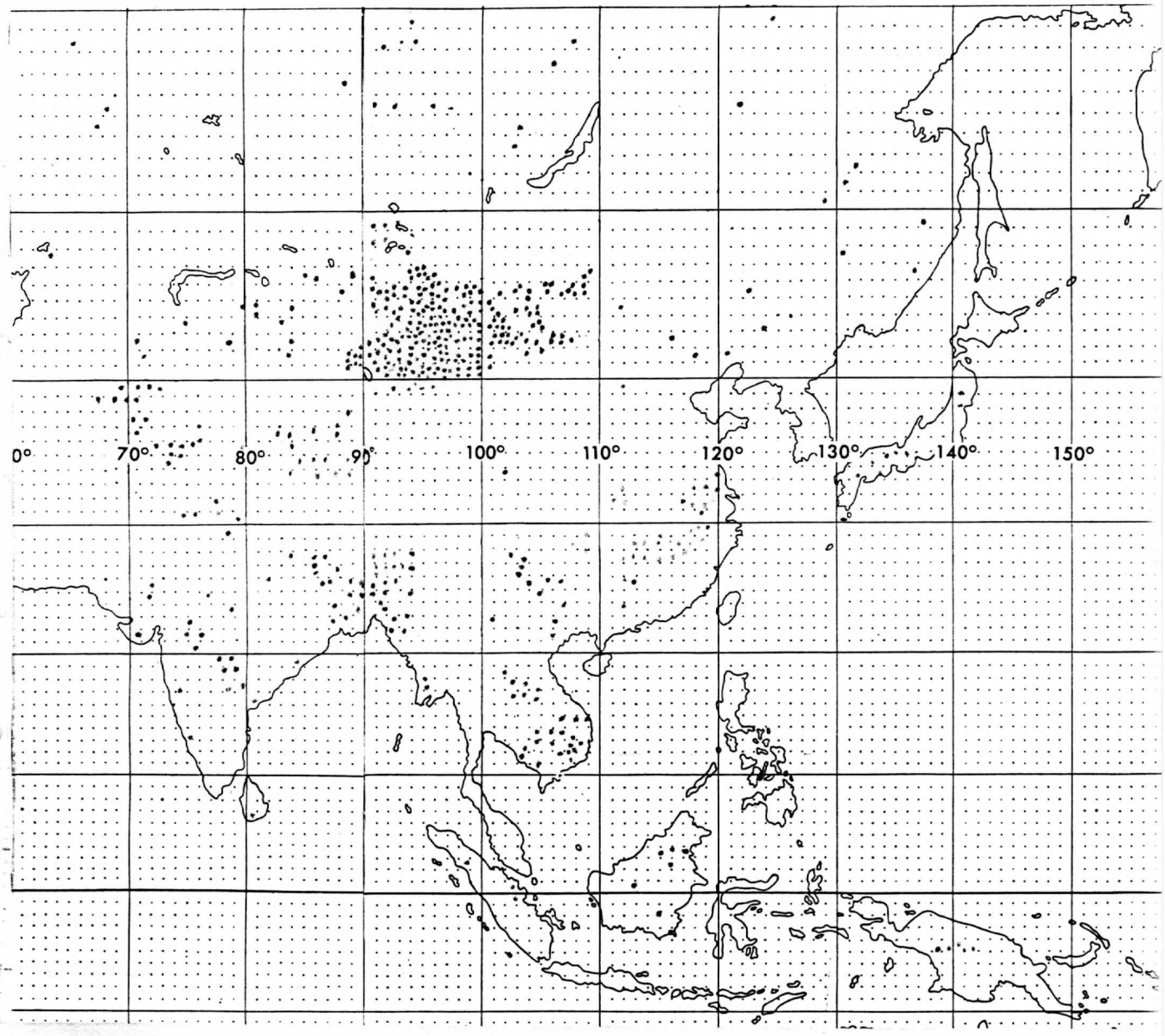

Fig. 1

Fig. 2 a) The soil distribution map of the Gobi Desert, and b) legend for the map. Dotted areas in blue represent areas of gobi (gravel).


乌鲁木齐市
天山
巴里坤哈萨克自治县
伊吾
哈密市
和静
焉耆回族自治县
库尔勒
博斯腾湖
阿克塔哈萨克族自治县
蒙古族自治县
45

Fig. 2a

沙漠沙丘活动程度类型
The Types to Extent of Sand Desert in Action.

裸露的流动沙丘（沙山）
Barren shifting dunes (megadunes).

快速移动的沙丘（＞10 米／年
Dunes moving with high speed (＞10m／yr)

中速移动的沙丘（＞5—10 米／年
Dunes moving with moderate speed (＞5—10m／yr)

慢速移动的沙丘及沙山（1—5 米／年
Dunes and megadunes moving with low speed (1—5m／yr)

极慢移动的沙山及沙丘（＜1 米／年
Megadunes and dunes moving with lowest speed (＜1m／yr)

植被复盖度中等的半固定沙丘
Semi-fixed dunes with moderate vegetative cover.

半固定沙丘
Semi-fixed dunes

植被复盖度较大的固定沙丘
Fixed dunes with thick vegetative cover.

固定沙丘
Fixed dunes

戈壁、绿洲
Gobi, oasis

戈壁（砾漠和石漠）
Gobi (gravel desert and rock desert)

绿洲
Oasis

沙漠地表形态类型
The types of sand desert landforms

以风积形态为主的沙丘及沙山
Dunes and megadunes — chiefly composed of wind-accumulated form.

新月形沙丘及沙丘链
Barchan dunes and barchan chains

格状沙丘链
Checkerboard dune chains

纵垄
Longitudinal dunes

羽毛状纵垄
Feather-like longitudinal dunes

树枝状纵垄
Dendritic longitudinal dunes

蜂窝状纵垄
Honeycomb longitudinal dunes

鱼鳞状沙丘
Scaled dunes

抛物线状沙丘
Paracolic dunes

蜂窝状沙丘
Honeycomb dunes on sandy ridges

蜂窝状沙丘
Honeycomb dunes

沙堆
Sand mounds

复合型穹状沙丘
Compound domes dunes

复合型链状沙丘及沙山
Compound transverse dunes a

复合型垄状沙丘及沙山
Compound longitudinal dunes and

金字塔沙丘及沙山
Pyramid dunes and megadunes

以风蚀形态为主的残丘
Yardan landforms — chiefly composed of wind-er

风蚀残丘
Wind-eroded yardang landform

Red = boundary-lines of natural Zones.

海岸沙丘
Coastal sand dunes

10 — 30 沙丘比高（米）
Relative height of dunes (m).

沙丘运动的主导方向
Prevailing directions of dunes

自然带界线
Boundary-lines of natural zones.

I 极端干旱地区
Hyperarid zone

II 干旱地区
Arid zone

III 半干旱地区
Semi-arid zone

IV 半湿润地区
Subhumid zone

比例尺 1:4000000

Fig. 2b

本图上中国国界线系按照地图出版社 1971 年

本图采用的投影：等面积圆锥投影
标准纬线 25°, 47°

Fig. 3 Images of SMMR vertically polarized brightness temperatures of the Gobi Desert at midnight at 37 GHz (a), 21 GHz (b), 18 GHz (c), 10.7 GHz (d), and 6.6 GHz (e). Brightness temperatures are coded as blue (lowest) to red (highest).

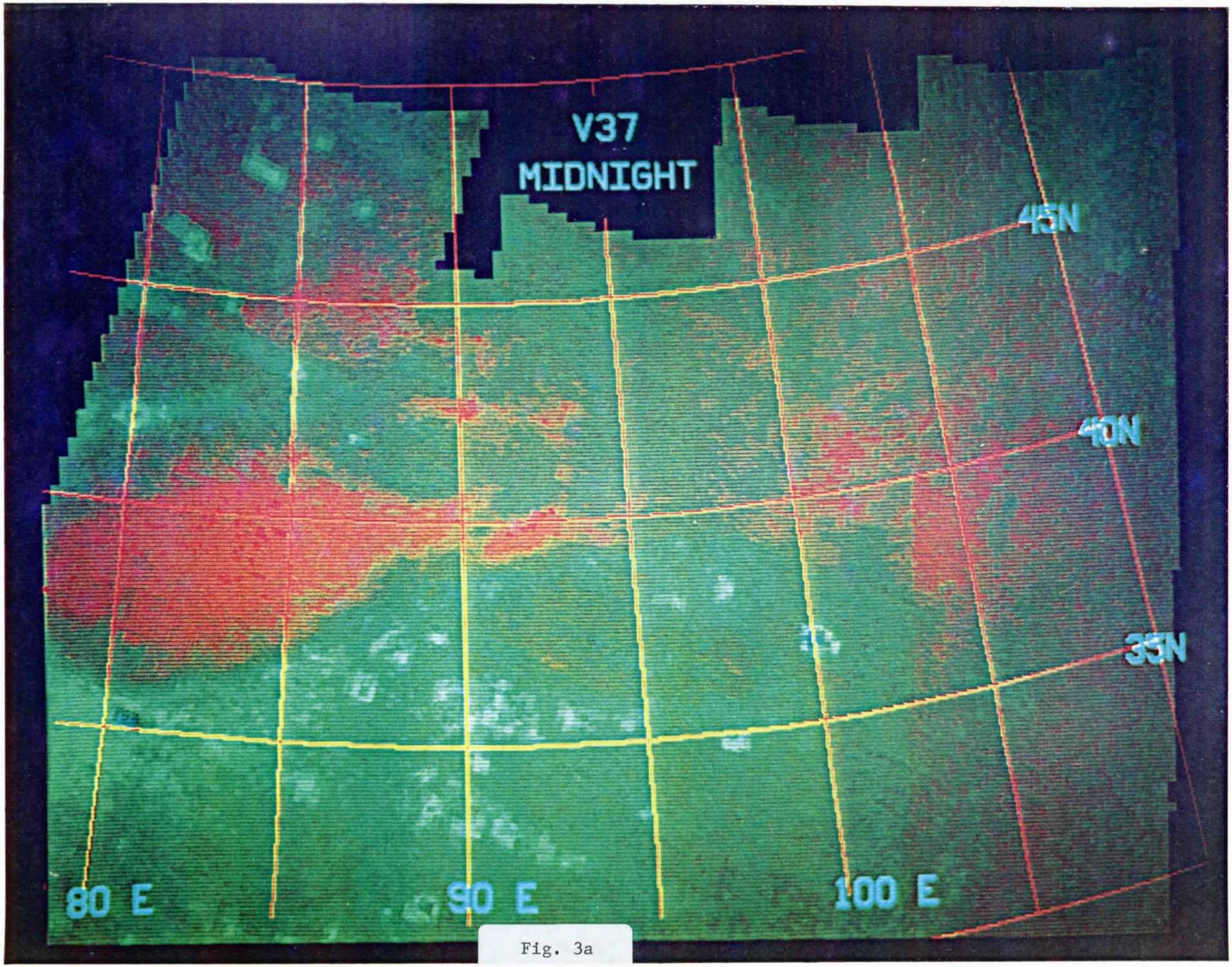

Fig. 3a

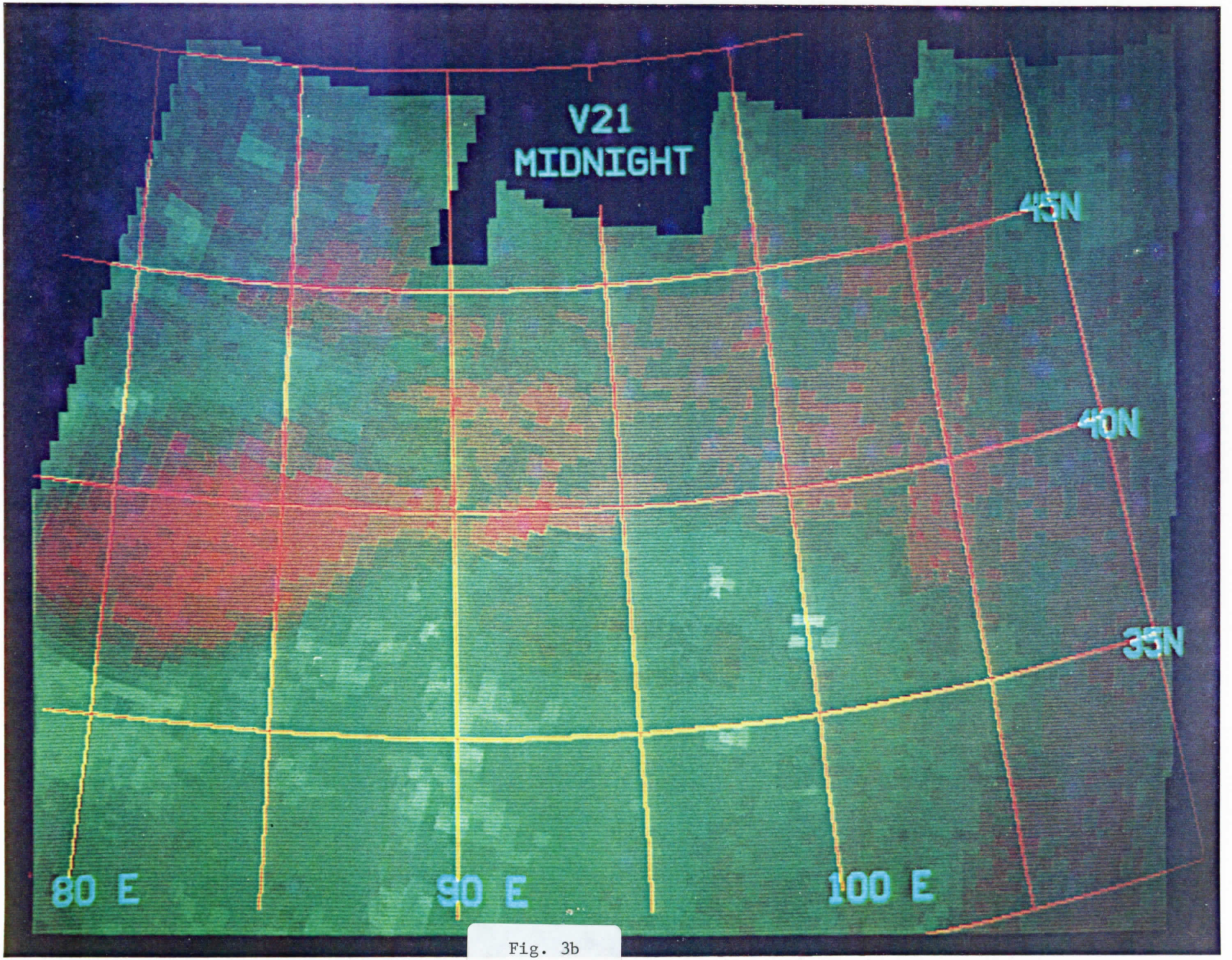

Fig. 3b

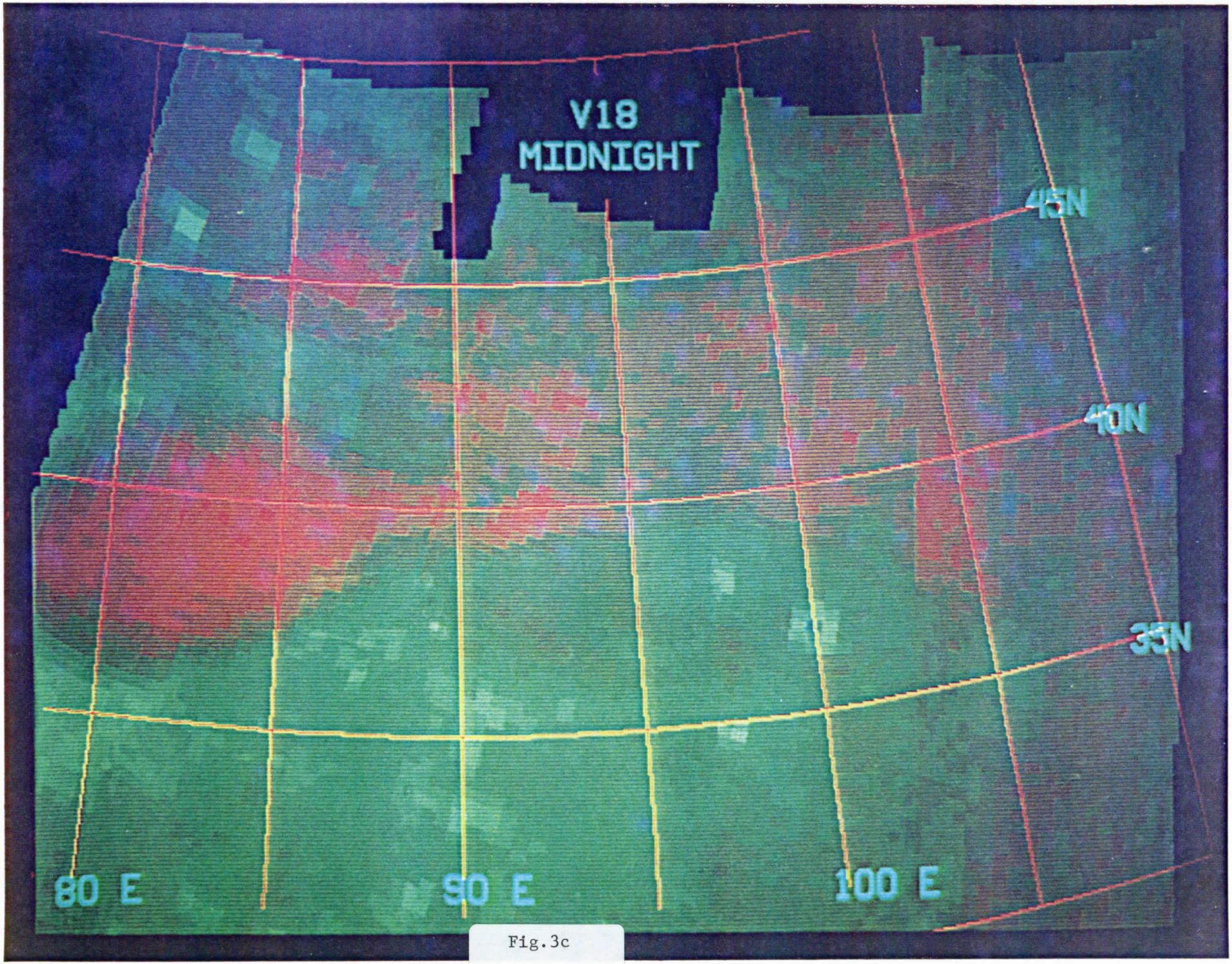

Fig.3c

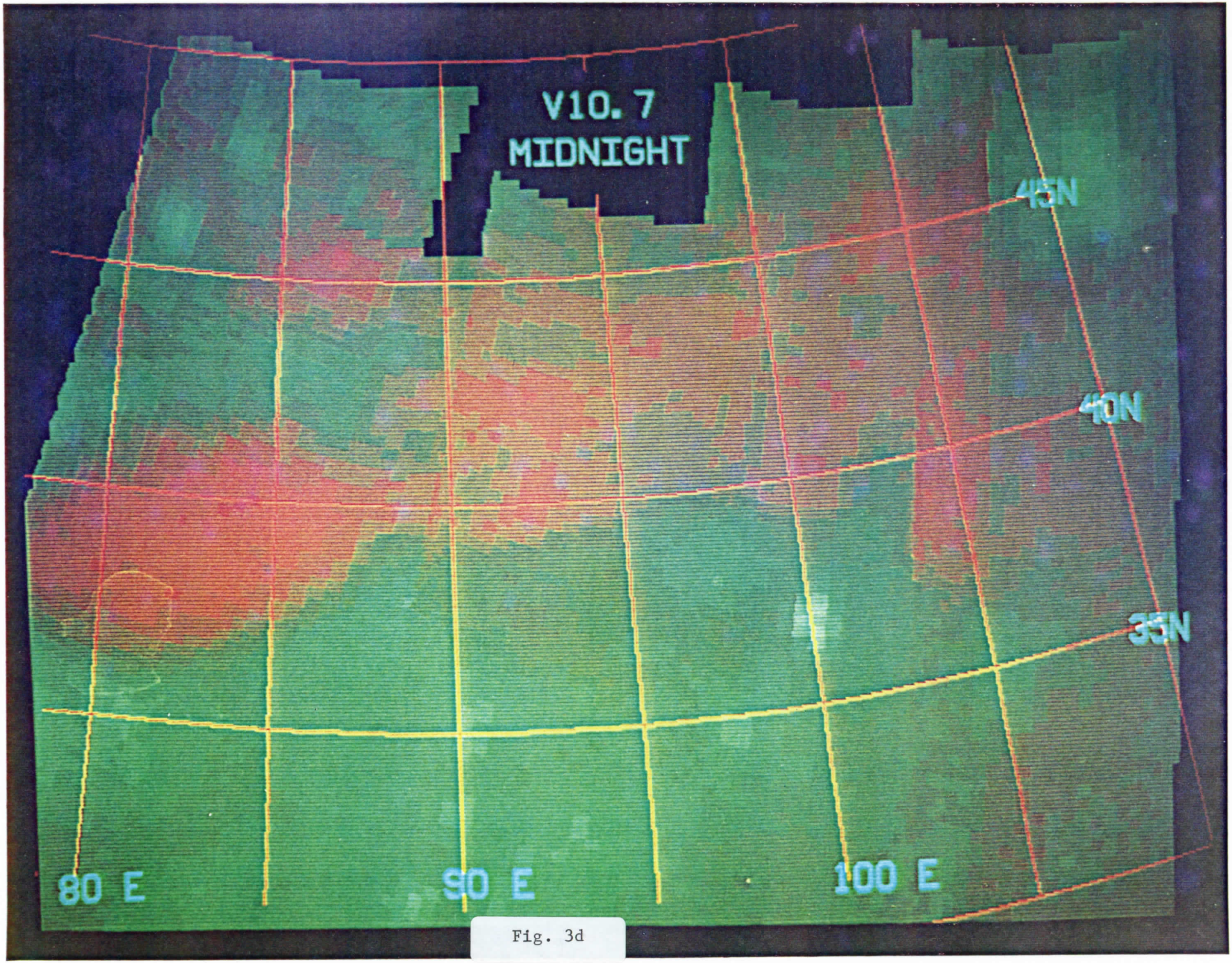

Fig. 3d

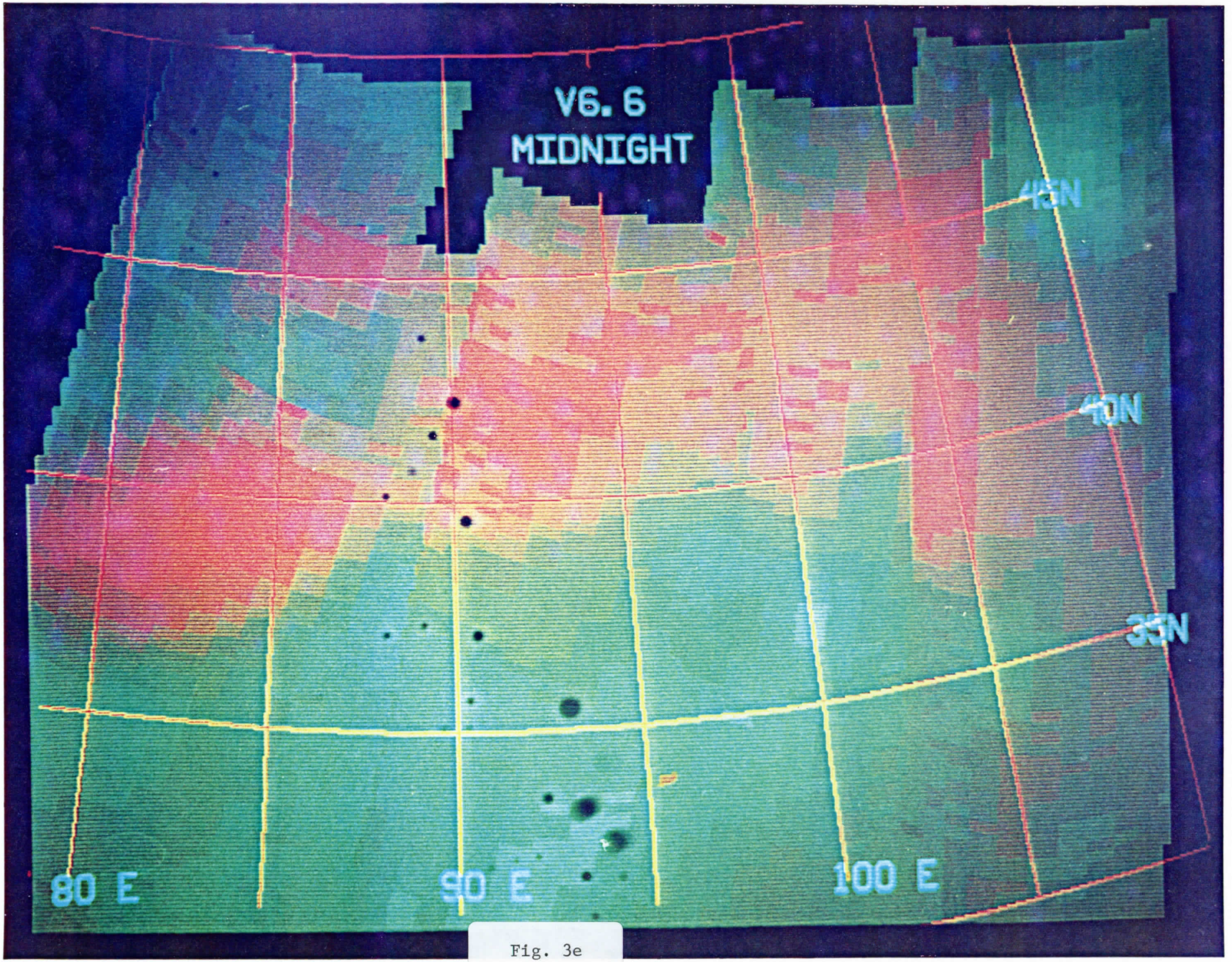

Fig. 3e

Fig. 4 Images of SMMR brightness temperature differences. In (a), the 37 GHz polarization image, values of V37-H37 are shown, where white represents polarizations of about 30°C, green (20°C), and red (10°C). In (b) the difference between the vertically polarized 37 and 21 GHz T_B's is shown (V21-V37) where white represents 8-10°C, green 4-7°C, and red 1-3°C. In (c), 21 GHz is replaced by 18 GHz.

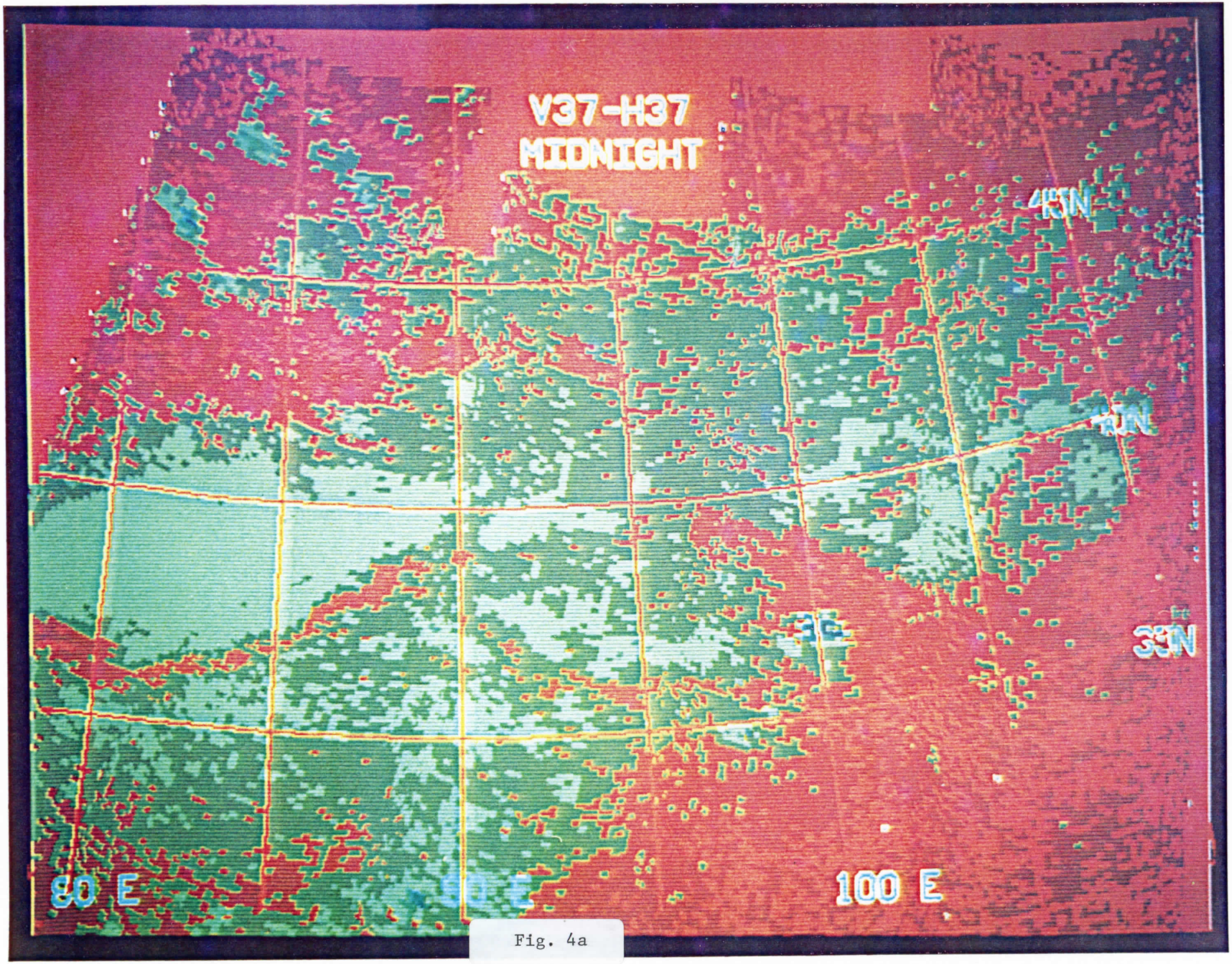

Fig. 4a

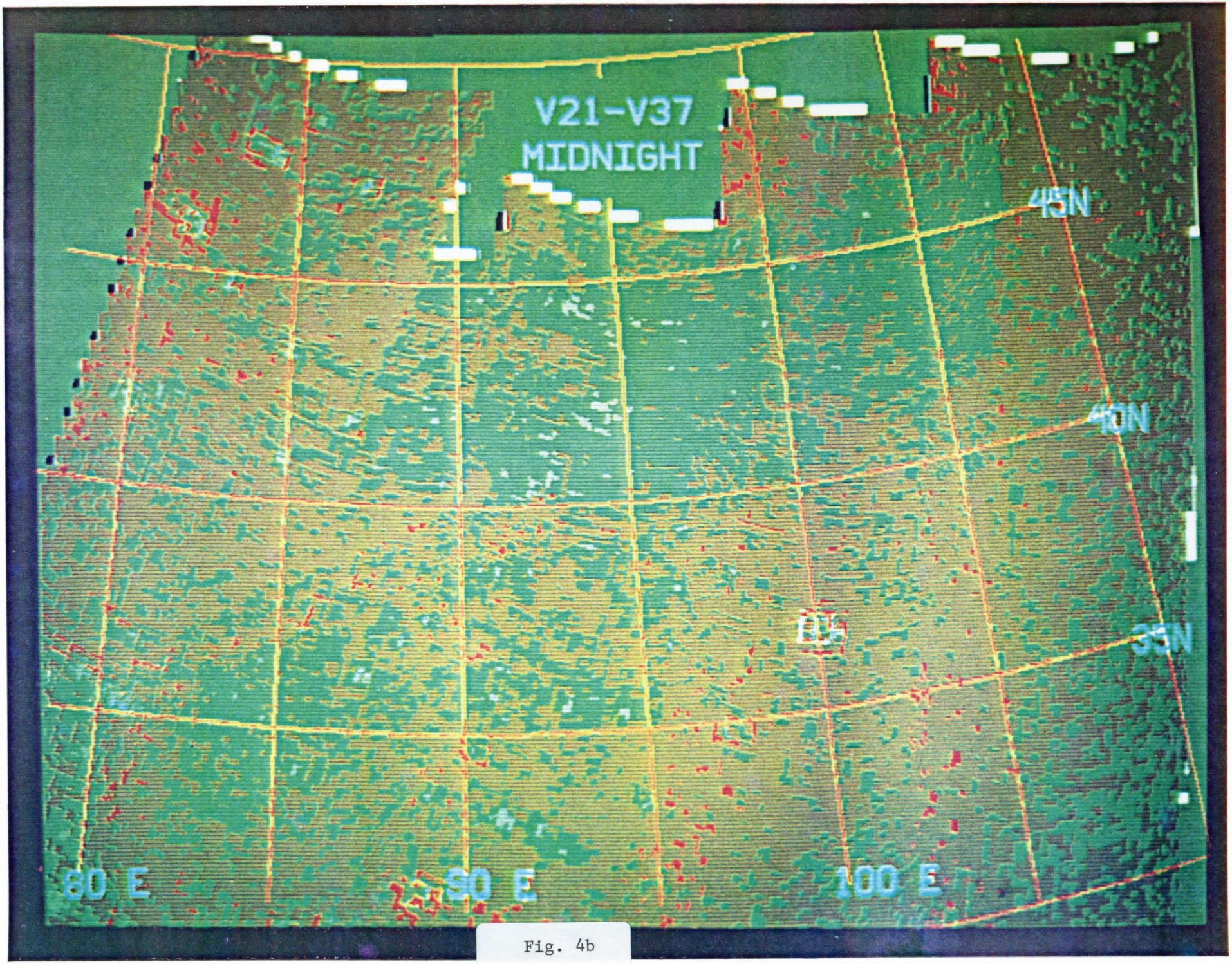

Fig. 4b

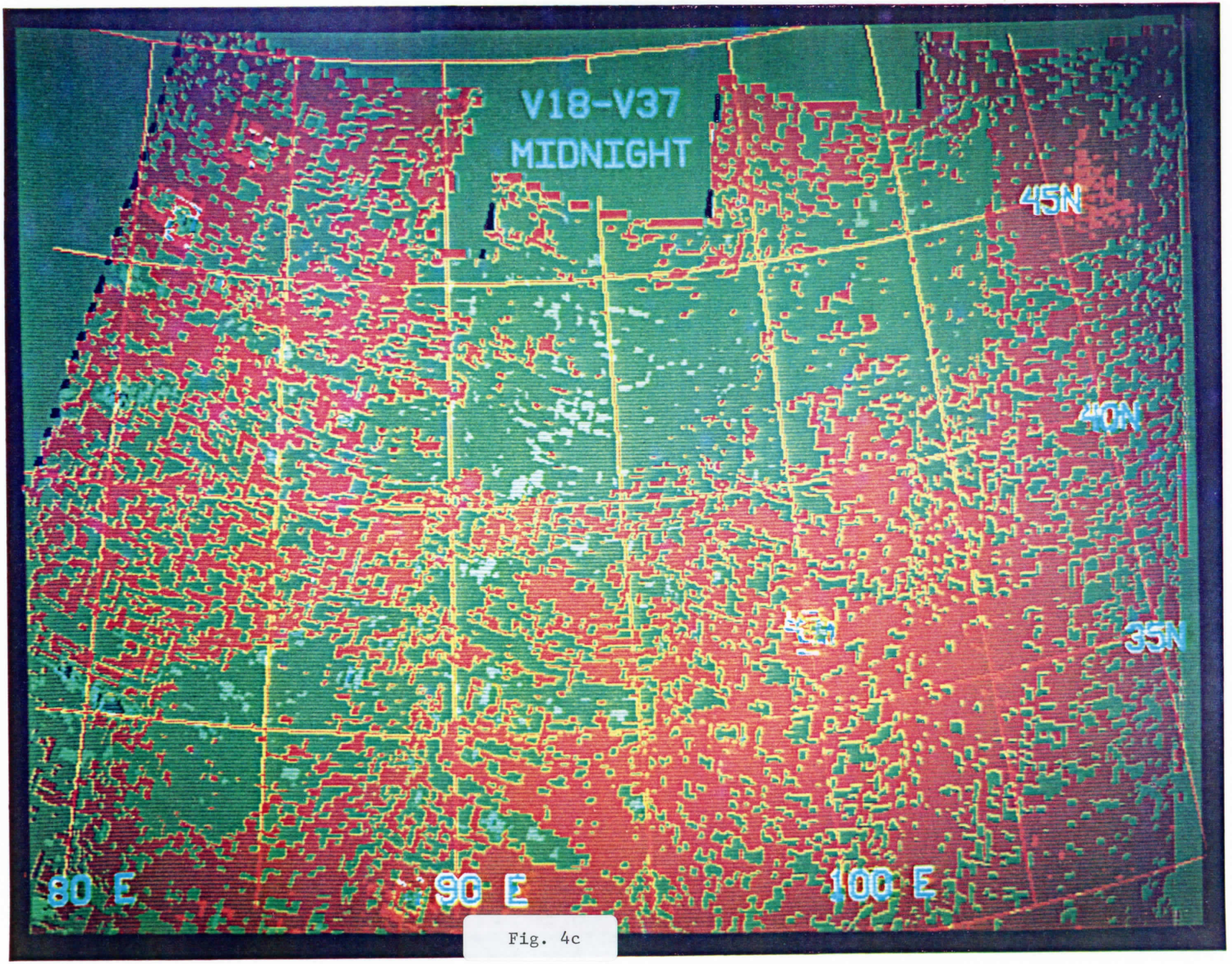

Fig. 4c

Fig. 5 Cross sections in longitude at midnight (a), at noon (b), and in latitude at midnight (c), and at noon (d), showing the geographical variation in average brightness temperature ($\overline{T}_B = (T_B{}^V + T_B{}^H)/2$) at all SMMR frequencies. Note that in (a) and (b), only in the Gobi desert does the 37 GHz T_B depart significantly from the other, lower frequency T_B's.


MIDNIGHT
37 GHZ
21
18
10.7
6.6
265
260
255
250
245
240
$\overline{T}_B$
sand DESERT
LOP NUR
GOBI
83°
84°
85°
86°
87°
88°
89°
90°
91°
92°
93°
94°
95°
96°
97°
98°
99°
100° E
(41° N)
LONGITUDE

Fig. 5a

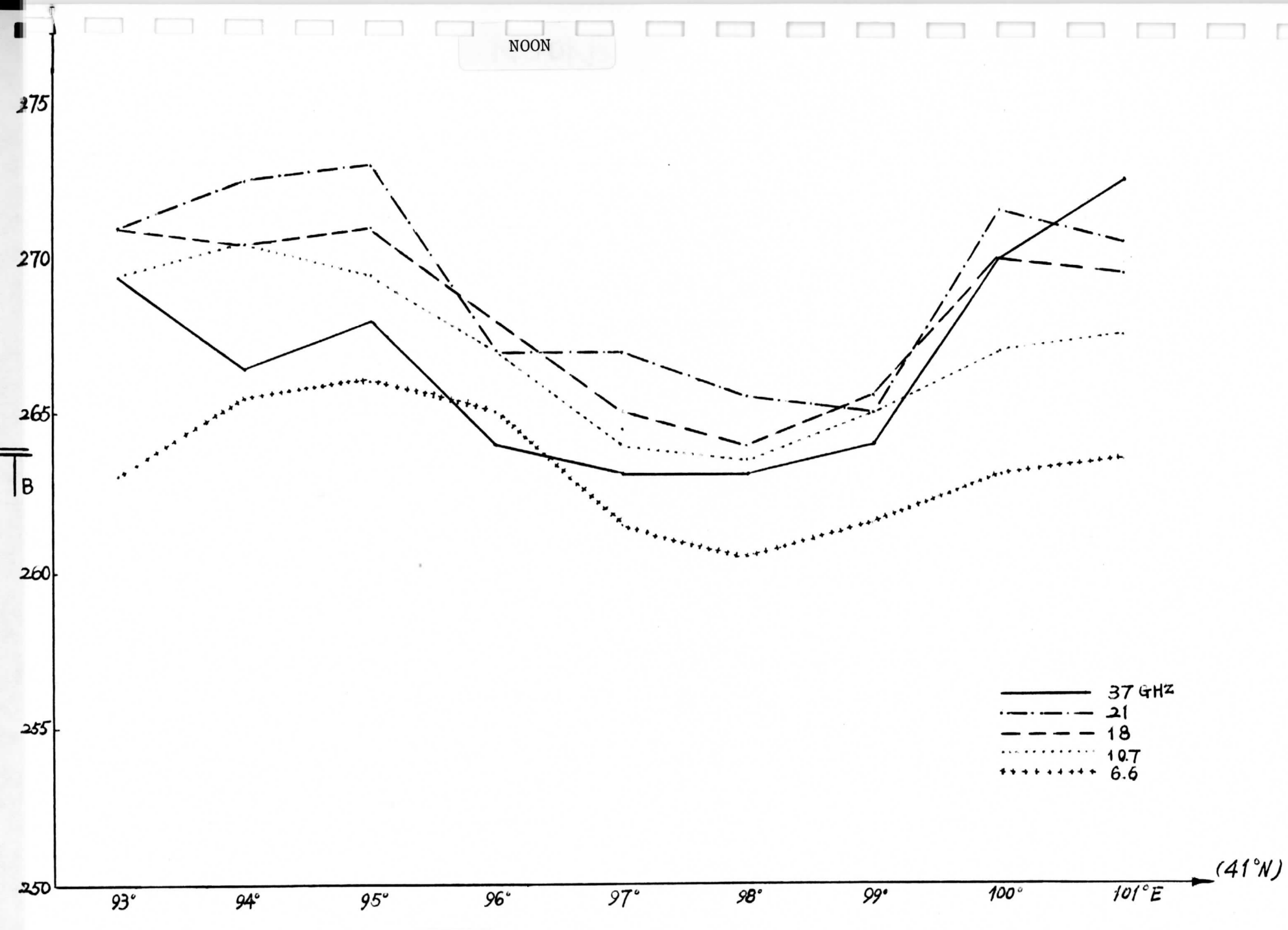
NOON
275
270
265
260
255
250
T
B
93°
94°
95°
96°
97°
98°
99°
100°
101°E
(41°N)
37 GHz
21
18
10.7
6.6
LONGITUDE

Fig. 5b

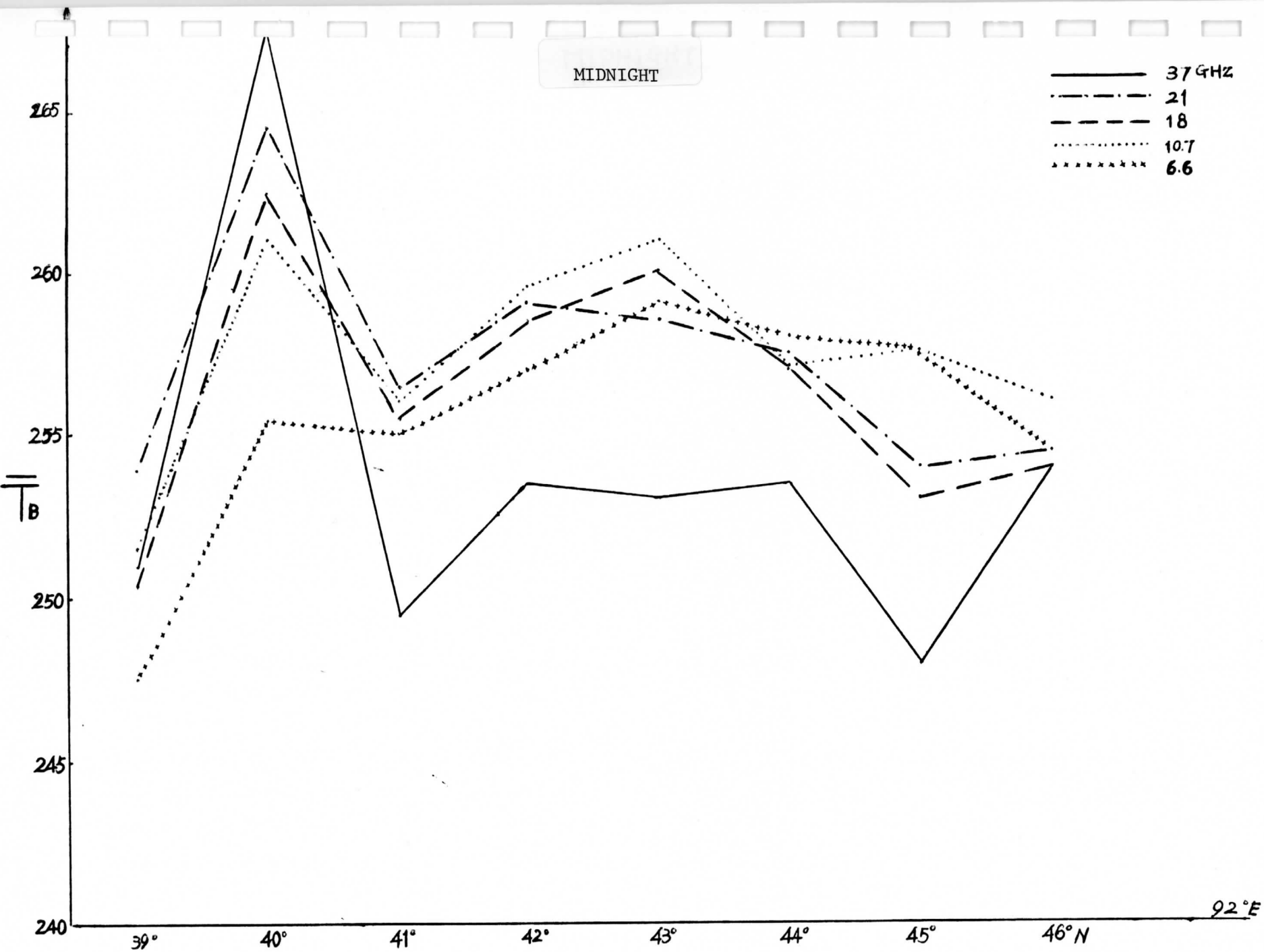
MIDNIGHT
37 GHz
21
18
10.7
6.6
265
260
255
250
245
240
$\overline{T}_B$
39°
40°
41°
42°
43°
44°
45°
46° N
92° E
LATITUDE

Fig. 5c

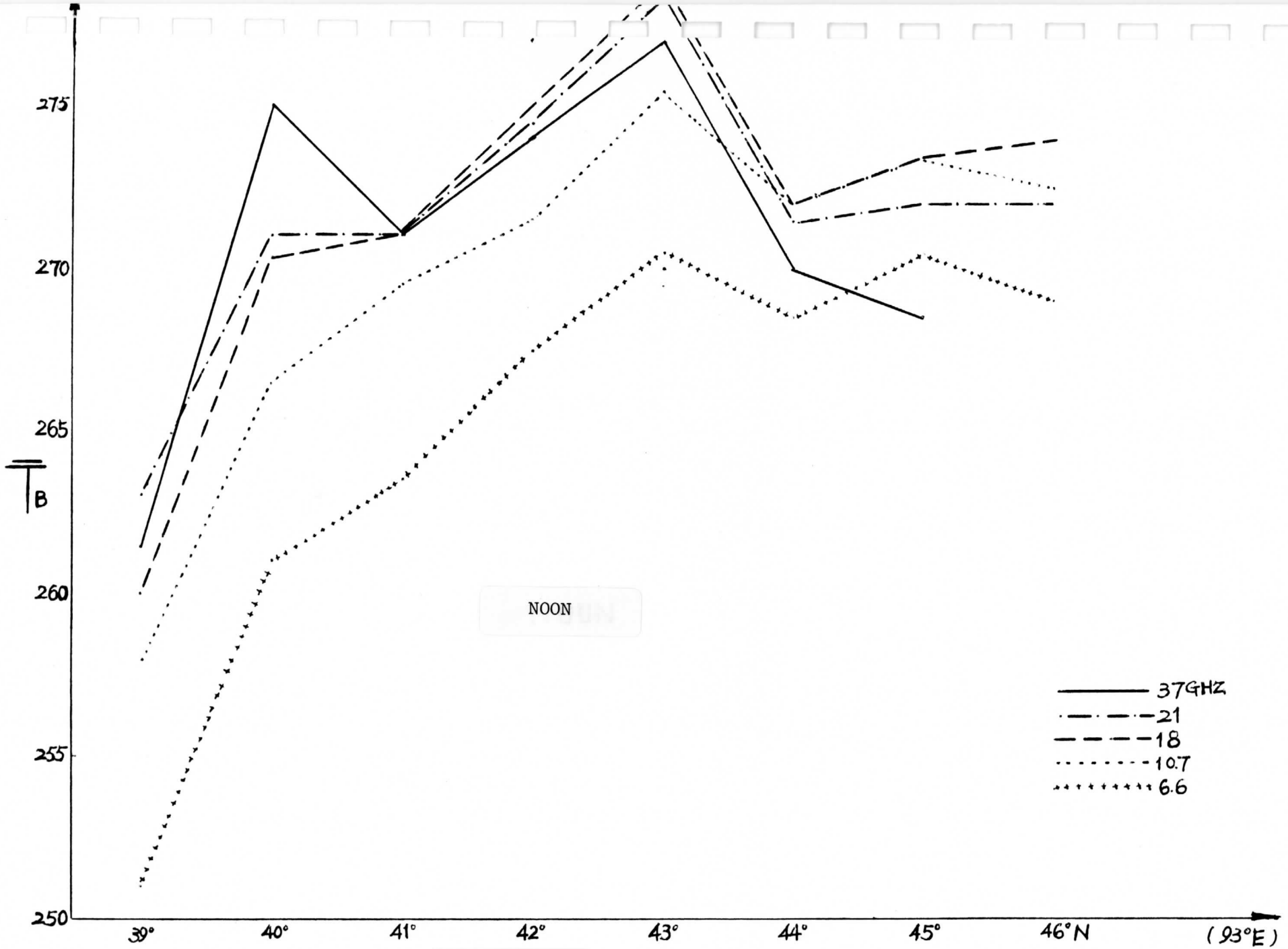
275
270
265
260
255
250
T_B
NOON
37GHZ
21
18
10.7
6.6
39°
40°
41°
42°
43°
44°
45°
46°N
(93°E)
LATITUDE

Fig. 5d

Fig. 6 SMMR images of

a) V21 - V37

b) (V18 + V21)/2 - V37

c) (V18 + H18)/2 - (V37 + H37)/2

d) V18 - V37

and e) (V6.6 + H6.6)/2 - (V37 + H37)/2

over the region 40° - 44°N, 89° - 96°E. These images show inter-frequency brightness temperature differences ranging from 0°C (black) to 10°C (white).

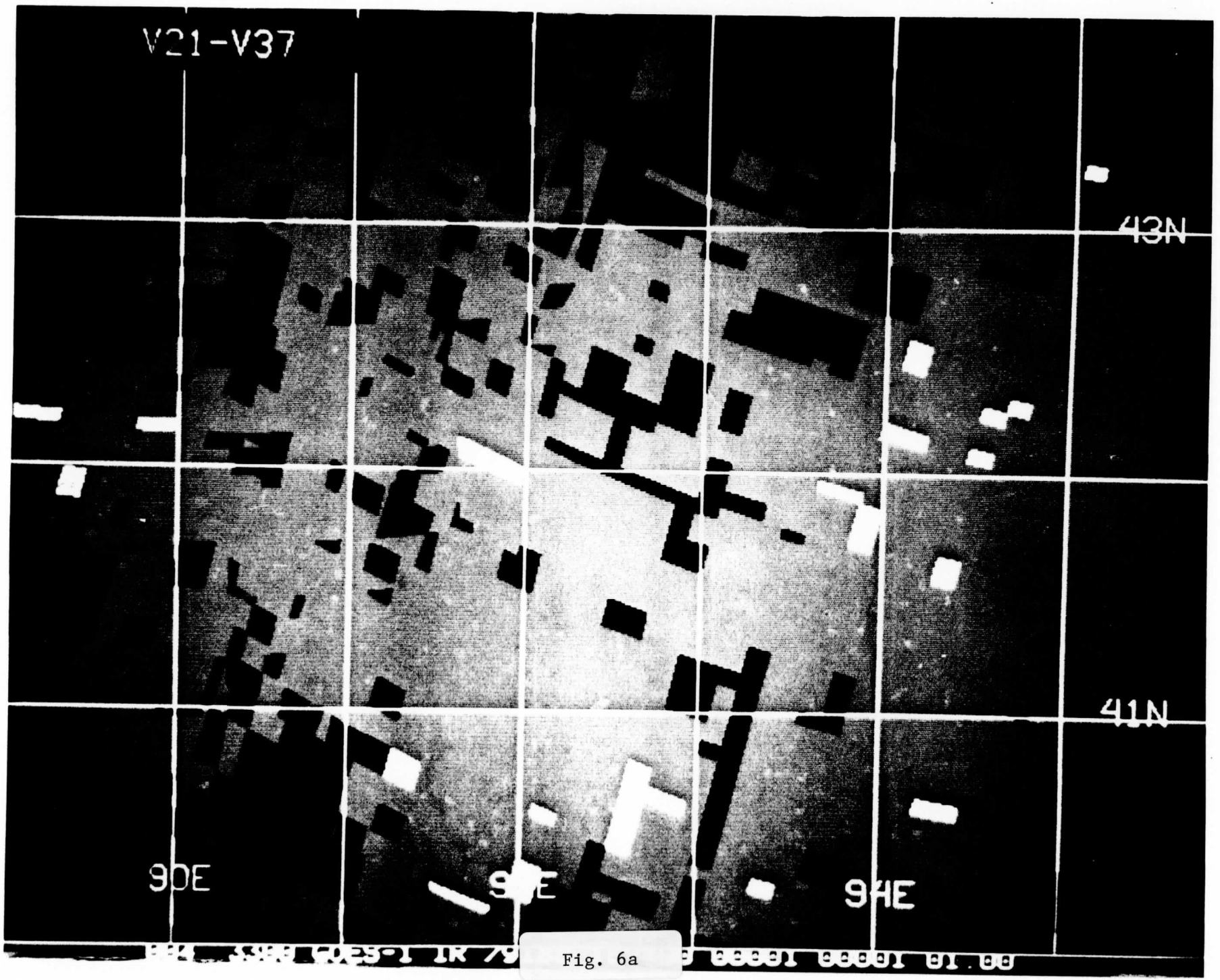

Fig. 6a

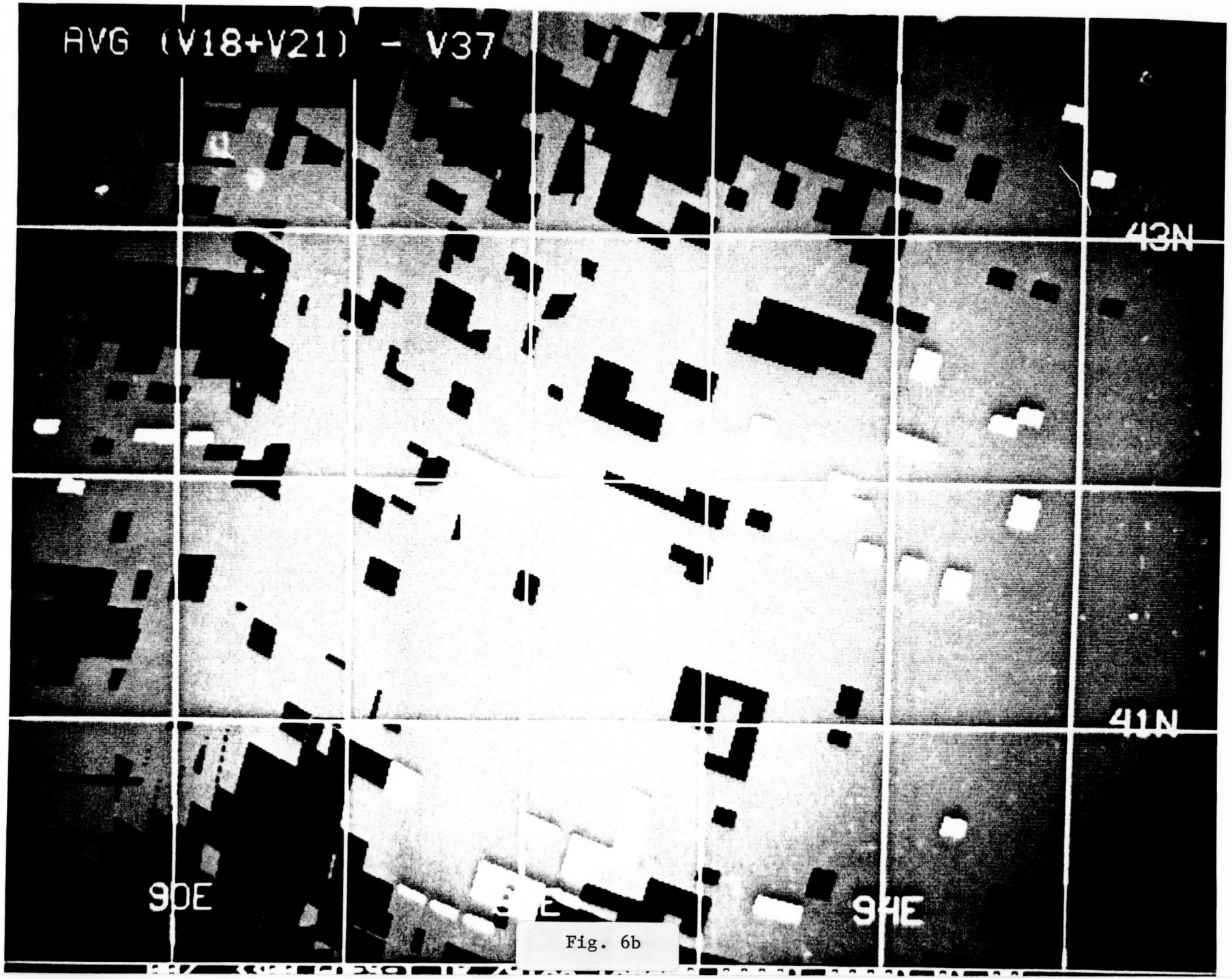

Fig. 6b

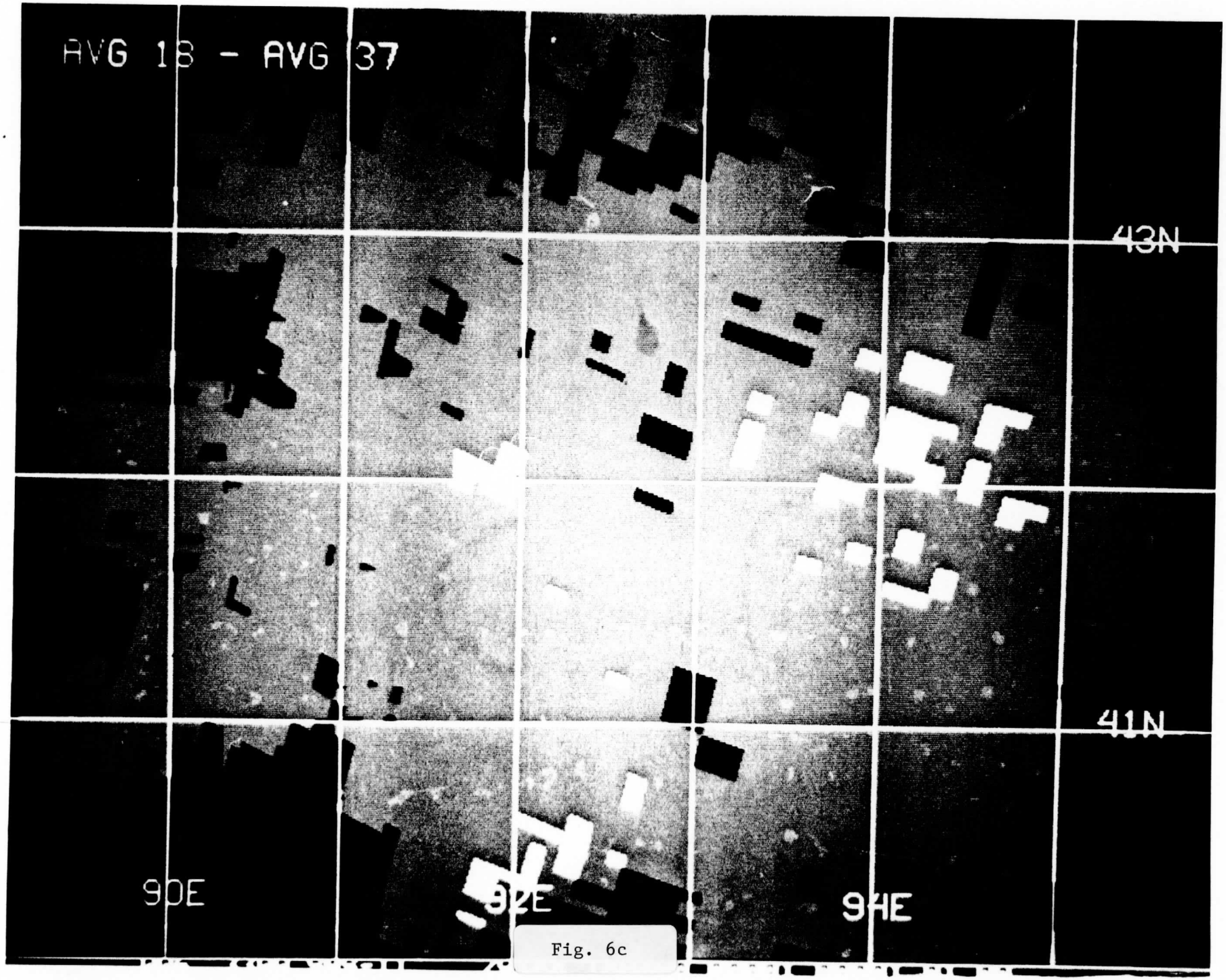

Fig. 6c

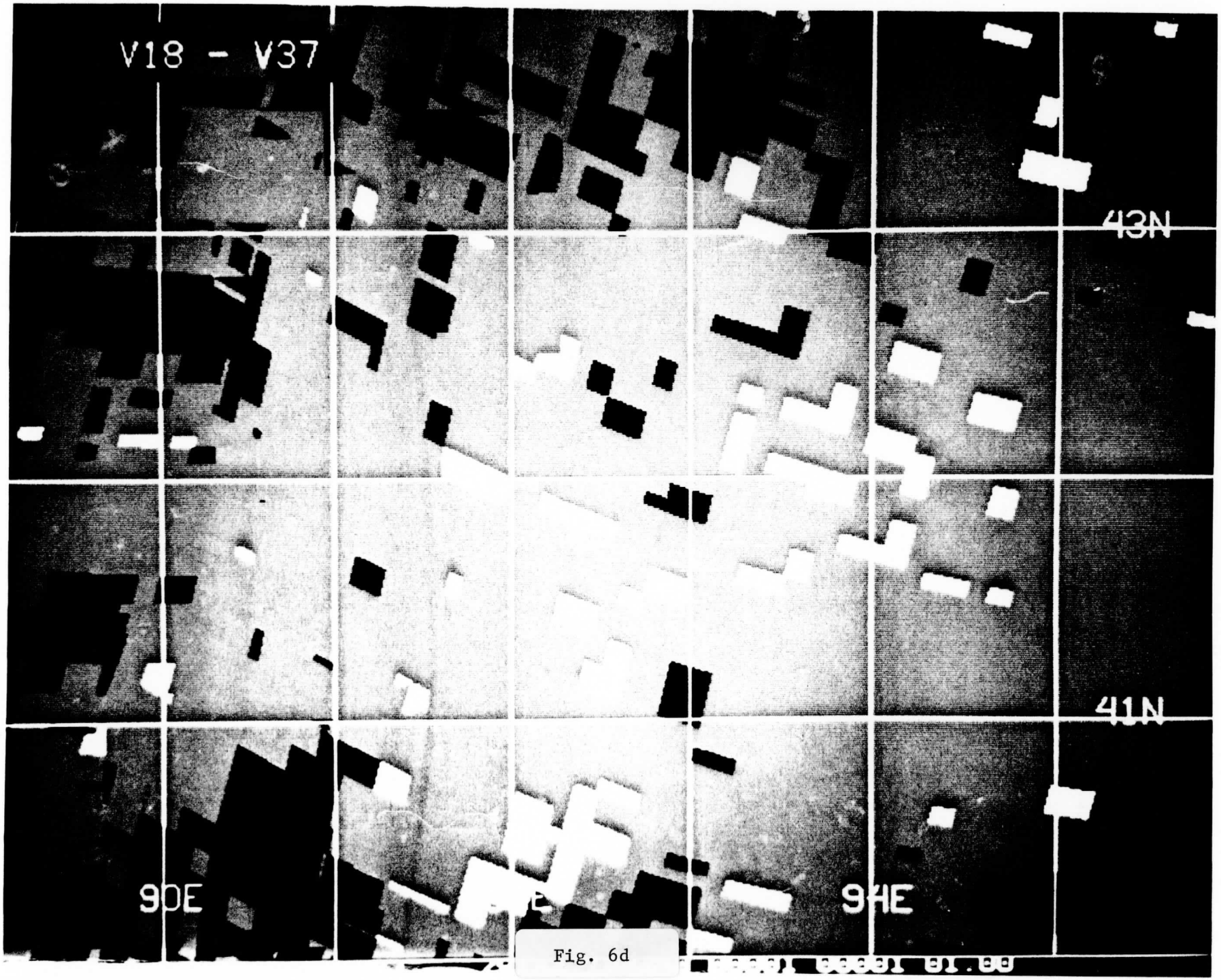

Fig. 6d

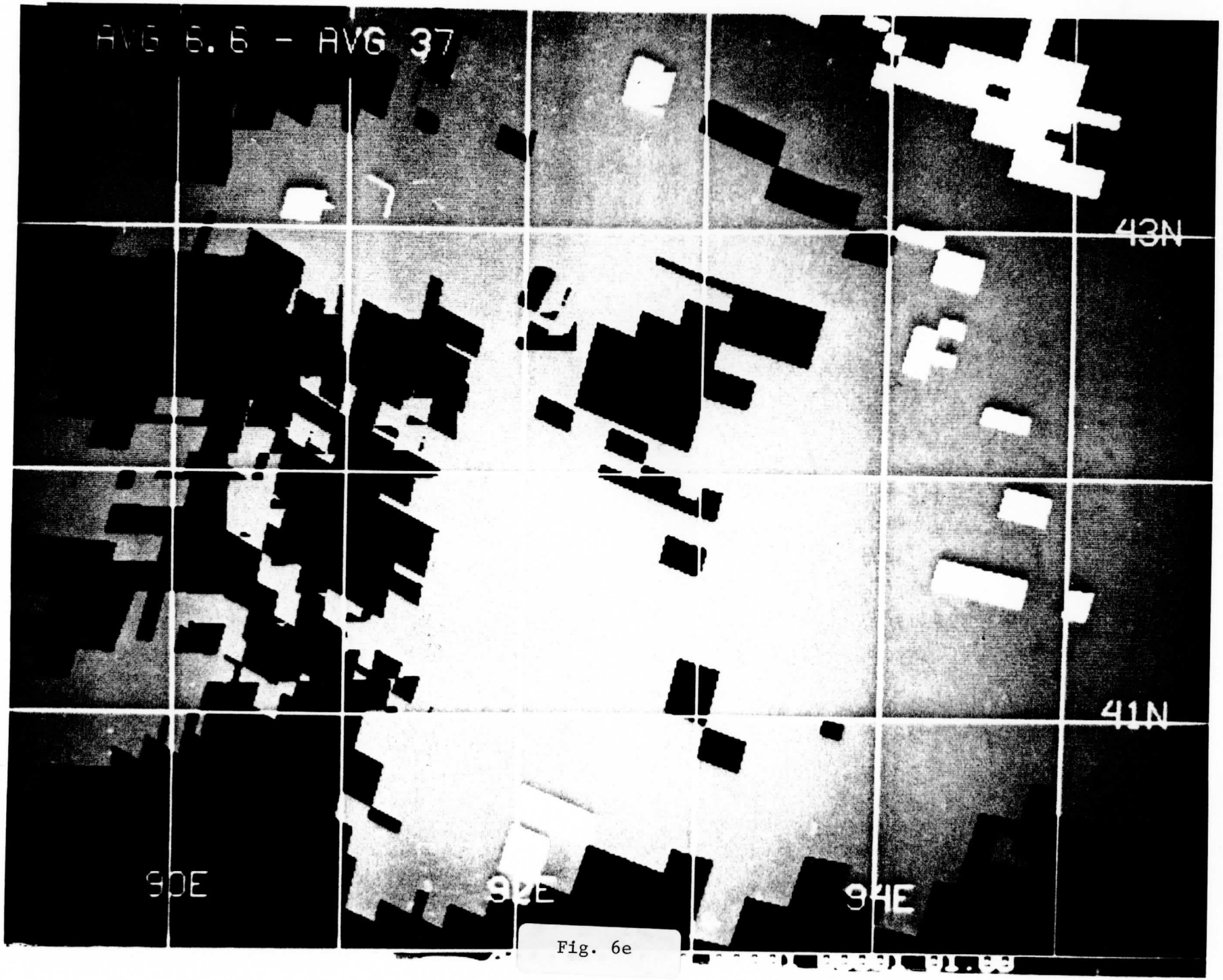

Fig. 6e